

## Aluminium-scandium tungstates solid solutions $\text{Al}_{2-x}\text{Sc}_x(\text{WO}_4)_3$ : Al and Sc distribution on a local scale

A. Yordanova<sup>1</sup>, S. Simova<sup>2</sup>, I. Koseva<sup>1</sup>, R. Nikolova<sup>3</sup>, V. Nikolov<sup>1</sup>, R. Stoyanova<sup>1\*</sup>

<sup>1</sup> Institute of General and Inorganic Chemistry, Bulgarian Academy of Sciences, Acad. G. Bonchev Str., Bldg. 11, Sofia 1113, Bulgaria

<sup>2</sup> Institute of Organic Chemistry with Centre of Phytochemistry, Bulgarian Academy of Sciences, Acad. G. Bonchev street, bl. 9, 1113 Sofia, Bulgaria

<sup>3</sup> Institute of Mineralogy and Crystallography "Acad. Ivan Kostov", Bulgarian Academy of Sciences, Acad. G. Bonchev street, bl. 107, 1113 Sofia, Bulgaria

Received April 27, 2017; Revised May 23, 2017

*Dedicated to Acad. Ivan Juchnovski on the occasion of his 80<sup>th</sup> birthday*

Multinuclear and multiple-quantum magic angle spinning (MQMAS) <sup>27</sup>Al and <sup>45</sup>Sc NMR spectroscopy and single crystal X-ray diffraction have been combined to assess and to quantify the distribution of Al and Sc on a local scale in mixed aluminium-scandium tungstates, which are of interest as materials with negative thermal expansion. The specific features of local cationic distribution have been studied by using  $\text{Al}_{2-x}\text{Sc}_x(\text{WO}_4)_3$  solid solutions ( $0 \leq x \leq 2$ ) in the form of single crystals and nano-powders. The <sup>27</sup>Al MAS and MQMAS NMR spectra indicate that Al atoms have two distinctly different coordination types in  $\text{Al}_{2-x}\text{Sc}_x(\text{WO}_4)_3$ . On the contrary, <sup>45</sup>Sc MAS and MQMAS NMR spectra display single coordination for Sc only. The crystal structure of  $\text{Al}_{2-x}\text{Sc}_x(\text{WO}_4)_3$  is revised to the orthorhombic space group  $P2_12_12_1$ , a non-isomorphic subgroup of  $Pbcn$ . In this structural model, there are two distinct non-equivalent Al/Sc positions: one of them is preferentially occupied by Al ions, while Sc ions reside at both positions. The coordination of Al and Sc in  $\text{Al}_{2-x}\text{Sc}_x(\text{WO}_4)_3$  is an intrinsic property, not depending on the form of  $\text{Al}_{2-x}\text{Sc}_x(\text{WO}_4)_3$  - single crystal or nano-powder.

**Key words:** Solid State NMR; Single Crystal X-ray Diffraction; Tungstates

### INTRODUCTION

Aluminium and scandium tungstates belong to a class of materials, which have a variety of functional properties that can easily be rationalized on the basis of their crystal structure. All members of the family  $\text{Me}_2(\text{WO}_4)_3$  crystallize in an orthorhombic space group [1–8]. The structure is composed of a three dimensional framework of corner-shared  $\text{MeO}_6$  octahedra and  $\text{WO}_4$  tetrahedra [9]. This type of linkage between cations ensures the structural flexibility, leading to the accommodation of metal ions with different sizes in the octahedral positions: the ionic radii of  $\text{Al}^{3+}$  and  $\text{Sc}^{3+}$  are 0.535 Å and 0.745 Å, respectively. The  $\text{Me}_2(\text{WO}_4)_3$  undergo a structure phase transition at temperatures, depending on the nature of the metal ion: -6 °C and -263 °C for  $\text{Al}_2(\text{WO}_4)_3$  and for  $\text{Sc}_2(\text{WO}_4)_3$ , respectively [10, 11]. The orthorhombic structure is easily transformed into a more dense monoclinic structure [12].

One approach to design the functional properties of tungstates comprises modelling of the structure by appropriate cationic substitution. This approach

is effective for improvement of the thermal expansion and optical properties of  $\text{Al}_{2-x}\text{Sc}_x(\text{WO}_4)_3$  solid solutions [7, 13–15]. Based on diffraction methods, it has been demonstrated that  $\text{Al}_2(\text{WO}_4)_3$  reacts with  $\text{Sc}_2(\text{WO}_4)_3$  forming solid solutions within the whole concentration range, the crystal structure being orthorhombic [16–18]. The solid solutions of  $\text{Al}_{2-x}\text{Sc}_x(\text{WO}_4)_3$  have been prepared in the form of single crystals and powders [16–18]. It is worth mentioning that growing of tungstate single crystals with defined compositions represents a difficult task by the Czochralski and the flux methods due to the volatility of  $\text{WO}_3$ , in the case of the first method and low growth rates and anisometric growth in the case of the flux method [16, 18]. Recently we have reported a new and facile method for the preparation of nano-powders  $\text{Al}_{2-x}\text{Sc}_x(\text{WO}_4)_3$  with defined composition varying from  $x=0$  to  $x=2$  [17]. The method consists in co-precipitation, followed by thermal treatment at 600°C using short heating time.

Although the properties of the individual compounds  $\text{Al}_2(\text{WO}_4)_3$  and  $\text{Al}_{2-x}\text{Sc}_x(\text{WO}_4)_3$  have been validated by many research groups, the properties of  $\text{Al}_{2-x}\text{Sc}_x(\text{WO}_4)_3$  solid solutions are still

\* To whom all correspondence should be sent:  
E-mail: radstoy@svr.igic.bas.bg

under debate [19]. These discrepancies could be explained with structural peculiarities of solid solutions  $Al_{2-x}Sc_x(WO_4)_3$  occurring on a local scale level due to the big mismatch between the ionic radii of  $Al^{3+}$  and  $Sc^{3+}$  (more than 10%). To the best of our knowledge, the cationic substitution on a local scale has not been explored yet, despite the long-range structure of solid solutions has been determined both by single crystal and powder X-ray diffraction techniques [19, 20]. The desired method of choice to probe the local structure of  $Al_{2-x}Sc_x(WO_4)_3$  is solid state NMR spectroscopy. The mechanism of ionic conductivity of  $Sc_2(WO_4)_3$  and  $Sc_2(MoO_4)_3$  and their solid solutions has been examined in terms of  $^{45}Sc$  MAS NMR spectroscopy [21]. The formation of  $Al_2(WO_4)_3$  during the co-precipitation reaction is monitored by us using  $^{27}Al$  MAS NMR [22].

This contribution aims to assess the cationic distribution in  $Al_{2-x}Sc_x(WO_4)_3$  solid solutions on a local scale by means of solid state  $^{27}Al$  and  $^{45}Sc$  MQMAS NMR spectroscopy and single crystal X-ray diffraction analysis. Tungstates are investigated in form of both single crystals and nano-powders. These series are already characterized as solid solutions  $Al_{2-x}Sc_x(WO_4)_3$  by means of powder X-ray diffraction. The single crystal X-ray diffraction is used to refine the crystal structure of  $Al_{2-x}Sc_x(WO_4)_3$ . The complementary application of both multinuclear solid state NMR and single crystal X-ray diffraction represents a new approach for structural characterization of tungstates  $Me_2(WO_4)_3$  on a local scale.

## EXPERIMENTAL

The nano-sized powders of  $Al_{2-x}Sc_x(WO_4)_3$  ( $x = 0.5, 1.0, 1.5$ ) were obtained using the co-precipitation method. Each of the solid solutions was synthesized using two separate aqueous solutions: sodium tungstate, obtained by dissolving  $Na_2WO_4 \cdot 2H_2O$  (p.a.) reagent, and mixed aluminium-scandium solution containing  $Al(NO_3)_3 \cdot 9H_2O$  and  $Sc(NO_3)_3 \cdot 4H_2O$  (14.4 wt.% Sc). The ratio between the two solutions, as well as the Al-to-Sc ratio, corresponds to the stoichiometric composition. The details of synthesis procedure have been given elsewhere [17]. Well crystallized  $Al_{2-x}Sc_x(WO_4)_3$  as solid solutions with particle sizes varying between 10 and 70 nm are obtained by this method [17, 23].

Single crystals of pure tungstates and their solid solutions (used as references) were obtained in the present investigation by the high-temperature

method using top-seeded solution growth and slow cooling down. The solvent used in all experiments was 27.5 $Na_2O$ –72.5 $WO_3$  mol %. The initial solute concentration and Al-to-Sc ratio were chosen on the basis of our previous investigation on the solubility of the solute into the above-mentioned solvent and in view of the distribution coefficient of Sc and Al [18].

For the sake of simplicity,  $Al_{2-x}Sc_x(WO_4)_3$  compositions will be further on denoted as N-ASW and SC-ASW, where N and SC symbols identify nano-powders and single crystals. Fig. 1 shows the images of N-ASW and SC-ASW samples.

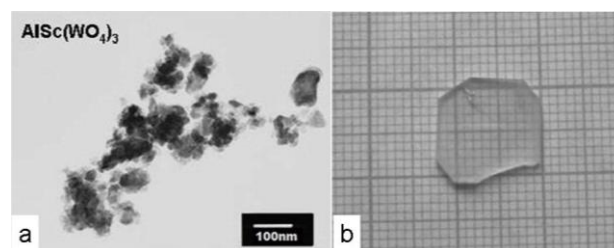


**Fig. 1.** TEM image of N-ASW (a) and optical image of SC-ASW (b).

Solid-state MAS  $^{27}Al$  and  $^{45}Sc$  NMR spectra were recorded at 156.4 MHz and 145.8 MHz on a Bruker AVII+ 600SB NMR spectrometer (magnetic field of 14.1 T). Single pulse excitation of 1  $\mu$ s, 0.2 s recycle delay and total number of scans of 1-2k were used. The samples were loaded into 4 mm zirconia rotors and spun at 9 and 14 kHz. Chemical shifts are quoted in parts per million, from external DSS (sodium 3-(trimethylsilyl)propane-1-sulfonate,  $\Xi$  scale).

3Q MQMAS  $^{27}Al$  and  $^{45}Sc$  NMR spectra were recorded at 130.3 MHz and 121.5 MHz on a Bruker HD 500SB NMR spectrometer (magnetic field of 11.7 T), using a 2.5 mm MAS probe. Samples were spun at 5 and 15 kHz using the 3- and 4-pulse z-filter pulse programs and the optimization procedure according to the Solids manual [24]. Experiments were obtained using rf-field strengths of 62.5 kHz for  $^{27}Al$  and 73.5 kHz for  $^{45}Sc$  with excitation and conversion pulses with lengths 4.0 (3.4)  $\mu$ s and 1.2 (0.9)  $\mu$ s and selective pulses of 18 (14)  $\mu$ s at 28 db lower intensity, respectively. Relaxation interval of 4-5 s, F2 spectral width of 105.6 ppm for both nuclei, 64 (80) time increments for F1 set to the rotor period and States-TPPI sign discrimination were used.

Structural characterization of nanopowders was carried out by powder X-ray diffraction using a Bruker D8 Advance powder diffractometer with  $Cu K\alpha$  radiation. Data were collected in the  $2\theta$  range

from 10 to 80 ° with a step of 0.04° and 1 s/step counting time. Concerning single crystal structure characterization, the intensity data were collected at room temperature by the  $\omega$ -scan technique on the Agilent Diffraction SuperNova Dual four-circle diffractometer, equipped with Atlas CCD detector, using mirror-monochromatized Mo-K $\alpha$  radiation from micro-focus source ( $\lambda=0.7107$  Å). The determination of cell parameters and the data processing procedure were performed by using the CrysAlis Pro program package [25]. The structure was solved by direct methods (SHELXS-97) and refined by full-matrix least-square procedures on F<sup>2</sup> (SHELXL-97) [26]. The structure visualization was performed by Crystal Maker (version 2.6.2, SN2080) [27]. The occupancies of Al and Sc in the mixed positions were refined simultaneously with the atomic coordinates and the atomic displacement parameters. The same isotropic or anisotropic displacement parameters are used for the atoms occupying the same position. Further details about the structure investigation may be obtained from Fachinformationszentrum (FIZ) Karlsruhe, under the CSD 429327 for *Pbcn* space group and CSD 429328 for *P2<sub>1</sub>2<sub>1</sub>2* space group.

## RESULTS AND DISCUSSION

### <sup>27</sup>Al and <sup>45</sup>Sc MQMAS NMR of $Al_{2-x}Sc_x(WO_4)_3$ solid solutions

Solid state <sup>27</sup>Al NMR spectroscopy was used aiming at the analysis of the structure of both single crystals and nano-powders  $Al_{2-x}Sc_x(WO_4)_3$  solid solutions by probing the Al local environment. Fig. 2 compares the <sup>27</sup>Al MAS NMR spectra for SC-ASW and N-ASW, where the amount of Al is varied from  $x=0$  to  $x=1.5$ . For the individual aluminium analogue, the <sup>27</sup>Al MAS NMR spectrum consists of a single resonance centred at about -4 ppm, the resonance position being the same for  $Al_2(WO_4)_3$  both in single crystals and nano-powders. The difference arises from the line width: the resonance of the single crystal is narrower than that of the nano-powder: 224 vs 294 Hz. This feature reveals the lower variation in the local coordination of Al in the case of the single crystal. Upon increasing the Sc content, a new resonance at -1 ppm, which is superimposed on the main resonance, grows up in its intensity. The resonance positions and line widths for the two signals are summarized in Table 1. The resonance positions of the two signals are independent of the Al-to-Sc ratio. The line widths of the intermediate compositions are similar and they are higher in

comparison with that of the individual composition. The only parameter, that is changing systematically with the Al-to-Sc ratio, is the resonance intensity (Table 1). Upon increasing the Sc content there is an increase in intensity of the signal centered at -1 ppm at the expense of the resonance at -4 ppm. This trend is observed for  $Al_{2-x}Sc_x(WO_4)_3$  both in the form of single crystals and nano-powders, thus indicating that the Al coordination in solid solutions of  $Al_{2-x}Sc_x(WO_4)_3$  is an intrinsic property.

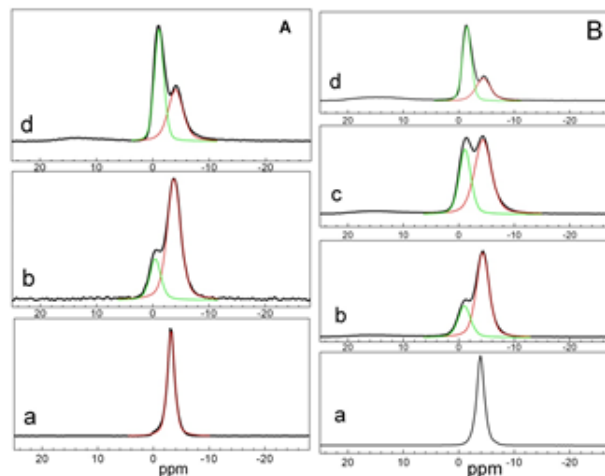


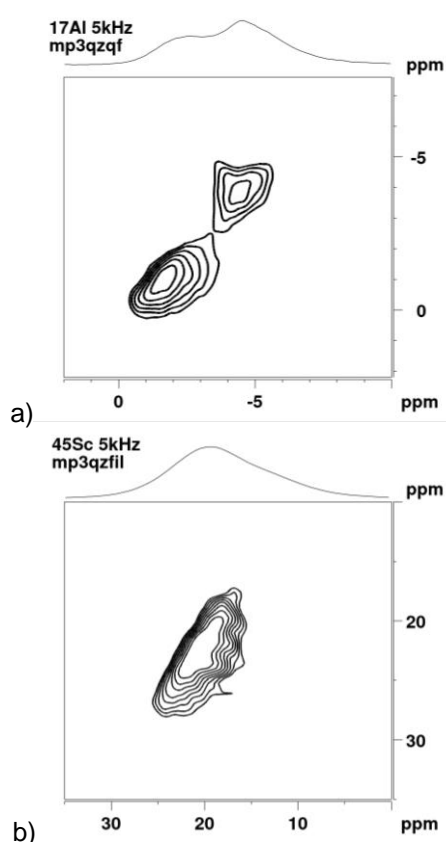
**Fig. 2.** <sup>27</sup>Al MAS NMR spectra of SC- $Al_{2-x}Sc_x(WO_4)_3$  (A) and N- $Al_{2-x}Sc_x(WO_4)_3$  (B):  $x=0$  (a);  $x=0.5$  (b);  $x=1.0$  (c) and  $x=1.5$  (d).

Because of the quadruple moment of Al, MQMAS NMR experiments were undertaken in order to increase the resolution of the <sup>27</sup>Al spectra. Fig. 3a shows the <sup>27</sup>Al MQMAS NMR spectrum. As one can see, there are two well separated signals. This means that MQMAS experiments confirm unambiguously the occurrence of two well defined coordinations of Al in  $Al_{2-x}Sc_x(WO_4)_3$  solid solutions.

Due to the larger quadrupole constant, the <sup>45</sup>Sc NMR spectra are usually broader and less resolved in comparison with that of <sup>27</sup>Al. However, the second order perturbation quadrupolar effects on the <sup>45</sup>Sc resonance line become negligible, when <sup>45</sup>Sc NMR spectra are registered at a stronger magnetic field (i.e. 11.7 T) [28]. That is why, the MAS NMR spectra are registered at a magnetic field of 14.1 T (Fig. 4). The <sup>45</sup>Sc NMR spectra of  $Al_{2-x}Sc_x(WO_4)_3$  solid solutions show broad resonance lines with centre of gravity at about 20 ppm (Fig. 4), in accordance with literature values for octahedrally coordinated Sc in  $Sc_2(WO_4)_3$ : 15.6 ppm and 9.3 ppm [21, 28]. The line widths of more than 1400 Hz are higher in comparison with these of <sup>27</sup>Al, which vary between 220 and 500 Hz.

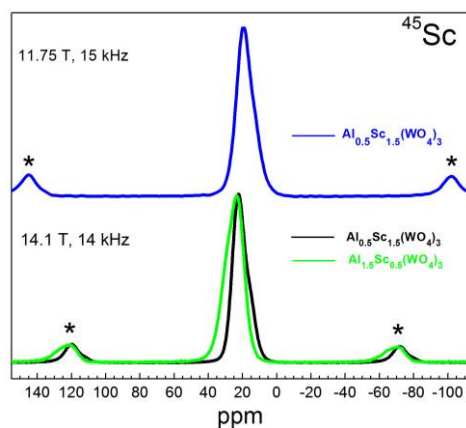
**Table 1.** Chemical shifts ( $\delta$ , ppm), line widths ( $\Delta\delta$ , Hz) and relative intensities of  $^{27}Al$  and  $^{45}Sc$  NMR signals in N-ASW and SC-ASW.

Samples	$^{27}Al$ Si1		$^{27}Al$ Si2		Relative part of $^{27}Al$ Si1	
	$\delta \pm 0.04$ , ppm	$\Delta$ , Hz	$\delta \pm 0.04$ , ppm	$\Delta$ , Hz	Si1	Si2
N-ASW, x = 0	-3.92	297			1.00	
N-ASW, x = 0.5	-4.02	403	-0.62	389	0.73	
N-ASW, x = 1.0	-4.48	494	-1.27	357	0.63	
N-ASW, x = 1.5	-4.07	446	-1.0	288	0.37	
SC-ASW, x = 0	-3.15	224			1.00	
SC-ASW, x = 0.5	-3.77	406	-0.45	333	0.78	
SC-ASW, x = 1.5	-4.02	452	-1.10	317	0.44	

**Fig. 3.** MQMAS spectra of  $^{27}Al$  (a) and  $^{45}Sc$  (b) in  $Al_{0.5}Sc_{1.5}(WO_4)_3$ .

The relatively weak quadrupolar moment of  $^{45}Sc$  allows acquisition of the spectra also at a magnetic field of 11.71 T, shown on the same figure. A broad line is also visible, which does not permit discrimination of the  $^{45}Sc$  atoms in different coordinations. Moreover, the center of gravity seems not to be dependent on the Sc content. The 4-pulse z-filter  $^{45}Sc$  3Q MQMAS NMR experiment was acquired for  $Al_{0.5}Sc_{1.5}(WO_4)_3$  (Fig. 3b). Contrary to the  $^{27}Al$  case, the  $^{45}Sc$  MQMAS spectrum displays only one signal with a dispersed shape. This

indicates that Sc atoms do not have distinct coordinations in solid solutions of  $Al_{2-x}Sc_x(WO_4)_3$ . This means that the main factor for the large line width is the distribution of  $^{45}Sc$  chemical shifts.

**Fig. 4.**  $^{45}Sc$  MAS NMR spectra of N-ASW:  $Al_{1.5}Sc_{0.5}(WO_4)_3$  (green lines) and  $Al_{0.5}Sc_{1.5}(WO_4)_3$  (black lines) registered at 14.1 T;  $Al_{0.5}Sc_{1.5}(WO_4)_3$  (blue lines) collected at 11.7 T.

The occurrence of dispersed MQMAS signals and broad MAS NMR signals can be related with smooth changes in the local coordination of Sc when Al is substituted for Sc, which is in agreement with a homogeneous distribution of  $^{45}Sc$  in  $Al_{2-x}Sc_x(WO_4)_3$  solid solutions.

The  $^{27}Al$  MAS NMR spectra clearly show that Al atoms have two distinctly different coordinations in  $Al_{2-x}Sc_x(WO_4)_3$  solid solutions, which is opposite to that for Sc. Taking into account that Al and Sc occupy only one crystallographic site in the orthorhombic crystal structure, the most obvious explanation is to associate the splitting of Al coordination with the effect of the neighbouring metal ions on the chemical shift. In the orthorhombic structure, every

$Al/ScO_6$ -octahedron shares common vertices with six  $WO_4$  tetrahedra, which, in their turn, are corner-connected with 18 Al/Sc ions. The small effect of the first W neighbours on the chemical shift of  $^{45}Sc$  has already been demonstrated for solid solutions of  $Sc_2(WO_4)_3$ - $Sc_2(MoO_4)_3$ , where a shift of about 5 ppm has been found during replacement of W by Mo [21, 28]. For the  $Al_{2-x}Sc_x(WO_4)_3$  solid solutions studied by us, we can expect a smaller effect of second Al/Sc neighbours on the chemical shifts of both  $^{27}Al$  and  $^{45}Sc$ . Although the  $W^{6+}$  and  $Mo^{6+}$  ions have similar ionic radii, the ionic mismatch for  $Al^{3+}$  and  $Sc^{3+}$  ions will create a more significant local distortion around the central Al/Sc nucleus, as a result of which a high variation in the chemical shift can be expected. On the other hand,  $Al^{3+}$  and  $Sc^{3+}$  neighbours are separated from the central Al/Sc nucleus at longer distances in comparison with that of W/Mo ions, which would create an opposite effect. Thus, the resonance at -4 ppm is attributed to Al nucleus having only  $Al^{3+}$  ions as first neighbours, while the resonance at -1 ppm originates from the Al nucleus surrounded mainly by  $Sc^{3+}$  ions. The negative shift of the resonance due to Al in  $Al^{3+}$  environment reveals that  $Al^{3+}$  neighbours create a stronger crystal field in comparison with that created by the  $Sc^{3+}$  ion neighbours. This is in agreement with the mean bond length Al/Sc-O in the two final compositions  $Al_2(WO_4)_3$  and  $Sc_2(WO_4)_3$ : 1.88 Å and 2.08 Å for Al-O and Sc-O, respectively [8]. Contrary to Al, the one  $^{45}Sc$  resonance can be attributed to Sc nucleus, whose metal surrounding is smoothly changed during progressive replacement of Al by Sc.

The next important feature is related with the type of Al/Sc distribution in  $Al_{2-x}Sc_x(WO_4)_3$  solid solutions. In accordance with our previous studies [17], all  $Al_{2-x}Sc_x(WO_4)_3$  crystallized in an orthorhombic space group, the lattice parameters being increased linearly with the Sc content. The Vegard dependence is also obeyed for tungstates  $Al_{2-x}Sc_x(WO_4)_3$  in the form of the single crystals [17]. The detection of two distinctly different coordinations of Al and only one coordination for Sc in the orthorhombic structure of  $Al_{2-x}Sc_x(WO_4)_3$ , ensuring only one crystallographic metal ion site, means that Al ions are not homogeneously distributed on a local scale in respect of Sc ions. On the other hand, the distances between Al/Sc nucleus and the  $Al^{3+}/Sc^{3+}$  neighbours are large (varying between 5.165 and 6.705 Å), which implies that non-homogeneous Al/Sc distribution is not a local phenomenon and it will cover domains with long sizes. At a first glance, it appears that NMR data

are in contradiction with the well described crystalline structure of  $Al_{2-x}Sc_x(WO_4)_3$  solid solutions [8, 17, 18].

#### Single crystal X-ray diffraction of $Al_{2-x}Sc_x(WO_4)_3$

In order to make NMR and crystalline structure data self-consistent, we reinvestigated the crystalline structure of  $Al_{2-x}Sc_x(WO_4)_3$  solid solutions in the form of single crystals. In the first approximation, the structure refinement is carried out within the framework of the structural model based on *Pbcn* space group. The refinement revealed that the chemical composition of the measured single-crystal sample is  $Al_{0.42}Sc_{1.58}(WO_4)_3$ , which is well consistent with the chemical analysis:  $Al_{0.40}Sc_{1.60}(WO_4)_3$  in accordance with EDAX analysis. At room temperature the studied compound is orthorhombic with lattice parameters and volume values quite similar to those observed for  $AlSc(WO_4)_3$  [4]. As it is expected the unit cell volume of the studied compound is larger than that of  $AlSc(WO_4)_3$  because of the higher Sc:Al ratio ( $V=1171\text{Å}^3$  versus  $1134\text{Å}^3$ , respectively). This is in agreement with data reported previously on the concentration dependence of the lattice parameters for  $Al_{2-x}Sc_x(WO_4)_3$  single crystals [16]. In addition, the lattice parameters for single crystal and nanopowder  $Al_{2-x}Sc_x(WO_4)_3$  with the same composition (i.e.  $x\sim 1.5$ ) are  $V=1171\text{Å}^3$  and  $V=1190\text{Å}^3$ , respectively.

Analyses of the structural similarity between each one of the end members and the studied solid solution have been performed by the program COMPSTRU at Bilbao Crystallographic Server. The measure of similarity ( $\Delta$ ) is defined as a function of the differences in atomic positions and the ratios between the corresponding lattice parameters of the structures [29, 30]. The calculated  $\Delta$ -value indicates that the crystalline structure of  $Al_{0.42}Sc_{1.58}(WO_4)_3$  is quite similar to that of  $Sc_2(WO_4)_3$  with  $\Delta = 0.004$ , while for the structure of  $Al_2(WO_4)_3$  this parameter is 0.014. The bond lengths Sc/Al – O vary in a slightly narrower range (from 1.999(5) to 2.050(4) Å) comparing with that in  $AlSc(WO_4)_3$  (1.997 – 2.055Å).

Taking into account that the crystalline structure of the solid solution is described in the *Pbcn* space group a statistical distribution of  $Al^{3+}$  and  $Sc^{3+}$  among one crystallographic site should be assumed. This also means that the W ions as first metal neighbours will only form one type of surrounding of Al (Sc) position. However, the NMR

spectroscopy proves clearly that Al and Sc ions occupy two distinctly different sites. Therefore, the next level of structure refinement is based on a model, where the structure of the solid solution is described in one of the maximal non-isomorphic subgroups of *Pbcn* space group where the M atomic position will be split into two symmetrically non-equivalent ones. There are four orthorhombic subgroups of space group *Pbcn* (60): *P2<sub>1</sub>2<sub>1</sub>2* (18), *Pca2<sub>1</sub>* (29), *Pnc2* (30) and *Pna2<sub>1</sub>* (33), respectively. Structure refinements in *P2<sub>1</sub>2<sub>1</sub>2* (18), *Pca2<sub>1</sub>* (29), *Pnc2*(30) and *Pna2<sub>1</sub>* (33) space groups have been tested using the experimental data obtained for the studied sample and the results are presented in Table 2. The refinement indicators are similar,

which makes difficult the assignment of the right space group. The values of the Flack parameter vary between 0.15 – 0.35, but only for *P2<sub>1</sub>2<sub>1</sub>2* and *Pca2<sub>1</sub>* space groups the uncertainty is relatively small. At first glance, this may indicate that the centrosymmetric space group is the correct one. However, it is worth mentioning that the value obtained for the Flack parameter is dependent on the Friedel coverage of the intensity data, approaching 0.5 for coverage of 100% and sticking near the starting value for coverage of 0%. For pseudo-centrosymmetric structures with heavy atoms in a centrosymmetric arrangement such as W, the obtained values of the Flack parameter are not strictly indicative (Table 2).

**Table 2.** Crystal data and structure refinement indicators for the studied composition, obtained for different space groups.

Space group	<i>P2<sub>1</sub>2<sub>1</sub>2</i> (18)	<i>Pca2<sub>1</sub></i> (29)	<i>Pnc2</i> (30)	<i>Pna2<sub>1</sub></i> (33)
Data/parameters	2861 / 158	2818 / 142	2757 / 158	2554 / 157
Goodness-of-fit on F <sup>2</sup>	1.025	0.970	1.136	1.136
Final R indices [ I > 2σ (I) ]	R = 0.0239 R <sub>w</sub> = 0.047	R = 0.0248 R <sub>w</sub> = 0.054	R = 0.0242, R <sub>w</sub> = 0.050	R = 0.0242, R <sub>w</sub> = 0.053
Final R indices (all data)	R = 0.0337 R <sub>w</sub> = 0.051	R = 0.0325 R <sub>w</sub> = 0.059	R = 0.0316 R <sub>w</sub> = 0.054	R = 0.0305 R <sub>w</sub> = 0.057
Largest difference peak and hole	1.21 and -1.562 eÅ <sup>3</sup>	1.308 and -1.322 eÅ <sup>3</sup>	1.390 and -1.473 eÅ <sup>3</sup>	1.107 and -1.982 eÅ <sup>3</sup>
Flack x *	0.33(5)	0.35(5)	0.14(7)	0.26(8)
Displacement parameters	Anisotropic for all atom	Two atoms non positive defined	Two atoms non positive defined	Two atoms non positive defined

**Table 3.** Atomic coordinates, Wyckoff positions and equivalent isotropic displacement parameters for  $Al_{0.42}Sc_{1.58}(WO_4)_3$ , refined in *P2<sub>1</sub>2<sub>1</sub>2*.

	Wyckoff positions	SOF	x	y	z	U(eq)
M1(Sc1)	4c	0.72(3)	0.2824(5)	0.3803(4)	0.5005(6)	0.0126(14)
M1(Al1)	4c	0.28(3)	0.2824(5)	0.3803(4)	0.5005(6)	0.0126(14)
M2(Sc2)	4c	0.94(3)	0.2157(4)	0.6192(3)	0.9984(6)	0.0113(12)
M2(Al2)	4c	0.06(3)	0.2157(4)	0.6192(3)	0.9984(6)	0.0113(12)
W11	4c	1	0.36743(11)	0.64432(9)	0.35520(15)	0.0178(3)
W12	4c	1	0.13216(11)	0.35573(9)	0.14571(15)	0.0179(3)
W21	2b	1	0	0.5	0.7230(2)	0.0173(4)
W22	2a	1	0.5	0.5	0.7773(2)	0.0170(4)
O11	4c	1	0.3219(18)	0.5255(11)	0.4320(2)	0.0370(5)
O12	4c	1	0.1780(14)	0.4743(10)	1.0740(2)	0.0290(5)
O21	4c	1	0.3367(16)	0.6457(12)	1.1718(19)	0.0370(5)
O22	4c	1	0.1549(15)	0.3624(12)	0.3300(17)	0.0260(4)
O31	4c	1	0.2430(2)	0.2368(12)	0.5680(2)	0.0350(5)
O32	4c	1	0.2640(2)	0.7581(11)	0.9290(3)	0.0390(5)
O41	4c	1	0.4520(12)	0.3298(11)	0.3890(2)	0.0280(4)
O42	4c	1	0.0434(14)	0.6668(13)	1.1110(2)	0.0410(5)
O51	4c	1	0.0819(16)	0.5922(11)	0.8340(2)	0.0280(4)
O52	4c	1	0.4095(16)	0.4136(13)	0.6720(2)	0.0340(4)
O61	4c	1	0.1273(16)	0.4374(14)	0.6120(3)	0.0450(5)
O62	4c	1	0.3837(15)	0.5653(14)	0.8810(3)	0.0450(5)

Among several proposed space groups, we choose the structural model based on  $P2_12_12$  space group since only refinement in this space group allows anisotropic description of the displacement parameters for all atoms. The atomic parameters of the studied compound in  $P2_12_12$  are represented in Table 3. In this model, there are two metal ions positions, which ensure different geometry for the metal ions (Table 4, Fig. 5). The refinement shows that Al atoms occupy preferentially one of the positions (marked with M1, Table 3 and 4), while Sc atoms reside in both positions (marked with M1 and M2, Table 3 and 4).

**Table 4.** Selected bond lengths (Å) of  $Al_{0.42}Sc_{1.58}(WO_4)_3$  refined in  $P2_12_12$ .

M1 – O61	1.956(17)	M2 – O32	1.986(15)
M1 – O31	2.017(16)	M2 – O21	2.026(15)
M1 – O22	2.025(17)	M2 – O51	2.034(17)
M1 – O41	2.032(15)	M2 – O42	2.046(16)
M1 – O11	2.040(16)	M2 – O12	2.056(15)
M1 – O52	2.062(18)	M2 – O62	2.066(17)

The preferential distribution of  $Al^{3+}$  among the two positions is consistent with the NMR data with splitting of Al lines in solid solutions of  $Al_{2-x}Sc_x(WO_4)_3$ . Due to the larger distance between Al/Sc ions, the effect of second metal neighbours can be neglected. This is supported by the experimental observations of the small effect of the first W and Mo neighbours on the chemical shift of  $^{45}Sc$ , as was observed previously [21, 28]. In addition, both  $^{27}Al$  and  $^{45}Sc$  NMR parameters are more sensitive towards the local coordination environment in comparison with the effect of metal neighbours. The resonance at -4 ppm can be attributed to Al occupying the second position, while Al in the first position causes the resonance shift at -1 ppm. In addition, the newly found refined structure can also answer the question why the only parameter that is systematically changing with the Al-to-Sc ratio is the  $^{27}Al$  NMR resonance intensity (relative intensities, Table 1). For  $Al_{2-x}Sc_x(WO_4)_3$  with  $x=1.5$ , the relative part of the NMR signal of  $^{27}Al$  at -4 ppm is 0.44 (Table 1), which is comparable with the relative part of Al in the M2-position determined from the crystal structure refinement: 0.06 (Table 3). The observation of one resonance signal for  $^{45}Sc$  is consistent with homogeneous distribution of Sc over two positions. These results demonstrate that  $^{27}Al$  MAS NMR

spectra allow quantification the distribution of Al over two crystallographic positions, established by single crystal X-ray diffraction (Table 1, Table 3).

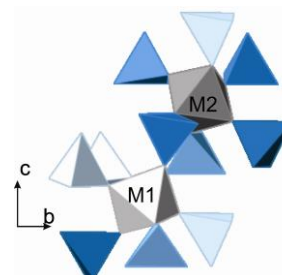


**Fig. 5** Detailed view of M1 and M2 positions in the  $P2_12_12$  space group.

## CONCLUSION

The crystalline structure of  $Al_{2-x}Sc_x(WO_4)_3$  solid solutions is being reconsidered. Single crystal X-ray diffraction shows that  $Al_{2-x}Sc_x(WO_4)_3$  solid solutions crystallize in an orthorhombic space group  $P2_12_12$ , which is a non-isomorphic subgroup of  $Pbcn$ . In this structural model, there are two symmetrically non-equivalent positions: one of them is preferentially occupied by Al, while Sc resides homogeneously both positions. The distribution of Al and Sc over crystallographic positions is monitored by multinuclear  $^{27}Al$  and  $^{45}Sc$  MAS and MQMAS NMR spectroscopy. The coordination of Al and Sc in  $Al_{2-x}Sc_x(WO_4)_3$  is an intrinsic property, which does not depend on the form of  $Al_{2-x}Sc_x(WO_4)_3$  whether it is single crystal or nano-powder. The local cationic distribution in  $Al_{2-x}Sc_x(WO_4)_3$  solid solutions can serve as a basis for reinterpretation of their thermal, conductive and optical properties.

**Acknowledgements:** The generous financial support of the Bulgarian Science Fund (projects UNA-17/2005, DRNF-02–13/2009 and DRNF-02–01/2009) is gratefully acknowledged.

## REFERENCES

1. T. Sugimoto, Y. Aoki, E. Niwa, T. Hashimoto, Y. Morito, *J. Ceramic Soc. Japan* **115**, 176 (2007).
2. J. S. O. Evans, T. A. Mary, A. W. Sleight, *J. Solid State Chem.*, **137**, 148 (1998).
3. Y. Okazaki, T. Ueda, S. Tamura, N. Imanaka, G. Adachi, *Solid State Ionics*, **136–137**, 437 (2000).
4. J. Zhu, J. Yang, X. Cheng, *Solid State Sci.*, **14**, 187 (2012).
5. Y. Zhou, S. Adams, R. Rao, D. Edwards, A. Neiman and N. Pestereva, *Chem. Mater.*, **20**, 6335 (2008).

6. K. Petermann, P. Mitzscherlich, *EEE J. Quantum Elect.*, **23**, 1122 (1987).
7. N. Dasgupta, E. Sörge, B. Butler, T.-C. Wen, D. K. Shetty, L. K. Cambrea, D. C. Harris, *J. Mater. Sci.*, **47**, 6286 (2012).
8. K. Nassau, H. J. Levinstein, G. M. Loiacono, *J. Phys. Chem. Solids*, **26**, 1805 (1965).
9. K. Nassau, *Rare Earth Res.*, **3**, 331 (1964).
10. V. E. Plyushev, V. M. Amosov, *Doklady Akademii nauk SSSR*, **157**, 131 (1964).
11. M. Maczka, K. Hermanowicz, J. Hanuza, *J. Mol. Struct.*, **744-747**, 283 (2005).
12. Y. Ogata, K. Tsuda, T. Hashimoto, *Japanese J. Appl. Phys.*, **47**, 4664 (2008).
13. J. S. O. Evans, T. A. Mary, A.W. Sleight, *J. Solid State Chem.*, **133**, 580 (1997).
14. M. Maczka, K. Hermanowicz, A. Pietraszko, A. Yordanova, I. Koseva, *Opt. Mater.*, **36**, 658 (2014).
15. J. Zhu, J. Yang, X. Cheng, *Solid State Sci.*, **14**, 187 (2012).
16. M. Hiraiwa, S. Tamura, N. Imanaka, G. Adachi, H. Dabkowska, A. Dabkowski, *Solid State Ionics*, **137**, 427 (2000).
17. A. Yordanova, I. Koseva, N. Velichkova, D. Kovacheva, D. Rabadjieva, V. Nikolov, *Mater. Res. Bull.*, **47**, 1544 (2012).
18. D. Ivanova, V. Nikolov, P. Peshev, *J. Crystal Growth*, **308**, 84 (2007).
19. C. Lind, *Materials*, **5**, 1125 (2012).
20. S. E. Ashbrook, *Phys. Chem. Chem. Phys.*, **11**, 6892 (2009).
21. N. Kim, J. Stebbins, *Chem. Mater.*, **21**, 309 (2009).
22. E. Zhecheva, R. Stoyanova, S. Ivanova, V. Nikolov, *Solid State Sci.s*, **12**, 2010 (2010).
23. D. Nihtianova, N. Velichkova, R. Nikolova, I. Koseva, A. Yordanova, V. Nikolov, *Mater. Res. Bull.*, **46**, 2125 (2011).
24. Bruker Solids User Manual, ver. 002, 2009.
25. Agilent. CrysAlis PRO (version 1.171.35.15). Agilent Technologies Ltd, Yarnton England, 2010.
26. G. M. Sheldrick, *Acta. Cryst. A*, **64**, 112 (2008).
27. Crystal Maker (version 2.6.2, SN2080).
28. S. Balamurugan, U. Ch. Rodewald, T. Harmening, L. Wüllen, D. Mohr, H. Eckert, R. Pöttgen, *Z. Naturforsch.*, **65b**, 13 (2010).
29. G. Bergerhoff, M. Berndt, K. Brandenburg, T. Degen, *Acta Cryst.*, **B55**, 147 (1999).
30. S. Parsons, H. D. Flack, T. Wagner, *Acta Cryst. B*, **69**, 249 (2013).

## ТВЪРДИ РАЗТВОРИ НА АЛУМИЕВО-СКАНДИЕВИ ВОЛФРАМАТИ $Al_{2-x}Sc_x(WO_4)_3$ : РАЗПРЕДЕЛЕНИЕ НА Al И Sc НА ЛОКАЛНО НИВО

A. Йорданова<sup>1</sup>, С. Симова<sup>2</sup>, Й. Косева<sup>1</sup>, Р. Николова<sup>3</sup>, В. Николов<sup>1</sup>, Р. Стоянова<sup>1\*</sup>

<sup>1</sup> Институт по обща и неорганична химия, Българска академия на науките, 1113 София, България

<sup>2</sup> Институт по органична химия с Център по фитохимия, Българска академия на науките, ул. Акад. Г. Бончев, бл. 9, 1113 София, България

<sup>3</sup> Институт по минералогия и кристалография „Акад. Иван Костов“, Българска академия на науките, ул. Акад. Г. Бончев, бл. 107, 1113 София, България

Постъпила на 27 април 2017 г.; Коригирана на 23 май 2017 г.

(Резюме)

За оценка на локалното разпределение на Al и Sc в смесени алуминиево-скандиеви волфраматни, интересни като материали с отрицателно термично разширение са използвани съвместно ЯМР метода „многоквантово възбуждане при въртене около магическия ъгъл“ (MQMAS) на ядрата  $^{27}Al$  и  $^{45}Sc$  и монокристална рентгенова дифракция. Изучаването на специфичните характеристики на локалното катионно разпределение е извършено на твърди разтвори  $Al_{2-x}Sc_x(WO_4)_3$  ( $0 \leq x \leq 2$ ) под формата на монокристали и нано-прахове. ЯМР спектрите на  $^{27}Al$  MAS и MQMAS показват, че Al атоми в твърдите разтвори на  $Al_{2-x}Sc_x(WO_4)_3$  приемат две ясно различаващи се една от друга координации. Обратно на Al атоми, ЯМР спектрите на  $^{45}Sc$  MAS и MQMAS дават указание само за една координация на Sc атоми. Кристалната структура на  $Al_{2-x}Sc_x(WO_4)_3$  е рафинирана в орторомбична симетрия с пространствена група  $P2_12_12$ , не-изоморфна подгрупа  $P6_{3c}$ . В този структурен модел се различават две нееквивалентни Al/Sc позиции: едната от тях е предпочитано заета от Al йони, докато Sc йони могат да заемат и двете позиции. Показано е, че координацията на Al и Sc във волфраматите е присъщо свойство за образците, което не зависи от формата им - монокристал или нанопрах.